

# Highly Monodisperse Zirconia-Coated Silica Spheres and Zirconia/Silica Hollow Spheres with Remarkable Textural Properties

Pablo M. Arnal, Claudia Weidenthaler, and Ferdi Schüth\*

Max-Planck-Institut für Kohlenforschung, Kaiser-Wilhelm-Platz 1, 45470 Mülheim an der Ruhr, Germany

Received November 22, 2005. Revised Manuscript Received February 9, 2006

High surface area zirconia is an interesting material for many applications. In this contribution, we describe the synthesis of  $\text{SiO}_2@\text{ZrO}_2$  and  $@\text{ZrO}_2$  (Liz-Marzán, L. M.; Correa-Duarte, M. A.; Pastoriza-Santos, I.; Mulvaney, P.; Ung, T.; Giersig, M.; Kotov, N. A. In *Handbook of Surfaces and Interfaces of Materials*; Nalwa, H. S., Ed.; Academic Press: San Diego, 2001; Vol. 3) of high surface area zirconia. The synthesis consists of (1) preparing monodisperse silica spheres; (2) coating the spheres with hydrated zirconia; (3) aging the composites; (4) calcining the composite at 1173 K; and (5) leaching the silica with NaOH solution. This process results in the formation of hollow zirconia spheres with a surface area of around  $300 \text{ m}^2 \text{ g}^{-1}$ . The zirconia is present in the tetragonal polymorph. The final material still contains silicon and sodium. However, it is present in a phase of which the nature could not be fully ascertained.

## Introduction

Materials with high surface area are an important field of research due to the many applications such materials find in catalysis, adsorption, and separation. While initially the research was predominantly focused on the generation of the high surface area materials themselves, now the synthesis often includes also the generation of desired macroscopic shapes. Considering the different morphologies targeted at, hollow spheres are among the most interesting ones, from a conceptual point of view with respect to applications, such as containers for controlled release.

Hollow spheres with a monodisperse size distribution are used in different fields of science. Hollow spheres with a low-index core and high-index shell are suitable for the preparation of photonic crystals with optical band gaps,<sup>2–6</sup> provided that the particles are monodisperse and have a smooth coating. In slow release applications, the spheres can be optimized for the target application, if control over sphere size and porosity of the shell is achieved. The flux of material out of the shell could then be controlled by structural factors, such as the thickness of the shell and the pore structure. Hollow spheres are also candidates for the preparation of materials with low density, filters, membrane supports, catalytic materials, and adsorbents.<sup>3,7</sup>

Monodisperse hollow spheres with sizes in the colloidal range are synthesized typically using a template sphere,<sup>8</sup> on

which the later shell is deposited. In most syntheses, the template is removed in a later step either by calcination or by dissolution.<sup>9,10</sup> These templates are normally inert, their only purpose is that of the scaffold to deposit the shell. There are few examples where the template reacts with the material of the shell. In these cases, the spherical cores do not only provide the scaffold for the formation of the shell, but the cores also contain and release a reactant needed for the formation of the shell.<sup>11</sup>

In general, the reported syntheses for monodisperse hollow spheres can be divided into four groups, according to the method used for creation of the shell. There are more methods to produce hollow spheres than those discussed in the following. However, these methods, such as spray-drying and dripping, emulsion, and suspension techniques, typically yield polydisperse hollow spheres instead of monodisperse spheres, which are the topic of this contribution.<sup>12,13</sup> The first group includes syntheses, where the template spheres are directly coated with a molecular precursor,<sup>14,15</sup> which is then converted to the solid on the template sphere. The second class resembles deposition-precipitation methods known for the formation of catalysts, where a surface-controlled precipitation is used to form directly nanoparticles of the desired solid on the template sphere.<sup>9,15,16</sup> The third method comprises syntheses using spherical particles with a nonporous core surrounded by a porous shell. This porous shell is then

\* Corresponding author. Tel.: +49 (0)208 306 2367. Fax: +49 (0)208 306 2995. E-mail: schueth@mpi-muelheim.mpg.de.

- (1) Liz-Marzán, L. M.; Correa-Duarte, M. A.; Pastoriza-Santos, I.; Mulvaney, P.; Ung, T.; Giersig, M.; Kotov, N. A. In *Handbook of Surfaces and Interfaces of Materials*; Nalwa, H. S., Ed.; Academic Press: San Diego, 2001; Vol. 3.
- (2) Holland, B. T.; Blanford, C. F.; Stein, A. *Science* **1998**, *281*, 538–540.
- (3) Imhof, A.; Pine, D. J. *Nature* **1997**, *389*, 948–951.
- (4) Wijnhoven, J.; Vos, W. L. *Science* **1998**, *281*, 802–804.
- (5) Xu, X. L.; Asher, S. A. *J. Am. Chem. Soc.* **2004**, *126*, 7940–7945.
- (6) Chen, Z.; Zhan, P.; Wang, Z. L.; Zhang, J. H.; Zhang, W. Y.; Ming, N. B.; Chan, C. T.; Sheng, P. *Adv. Mater.* **2004**, *16*, 417–422.
- (7) Imhof, A.; Pine, D. J. *Adv. Mater.* **1998**, *10*, 697–700.

- (8) Schüth, F. *Angew. Chem., Int. Ed.* **2003**, *42*, 3604–3622.
- (9) Sukhorukov, G. B.; Fery, A.; Brumen, M.; Mohwald, H. *Phys. Chem. Chem. Phys.* **2004**, *6*, 4078–4089.
- (10) Yoon, S. B.; Sohn, K.; Kim, J. Y.; Shin, C. H.; Yu, J. S.; Hyeon, T. *Adv. Mater.* **2002**, *14*, 19–21.
- (11) Wang, Y. L.; Cai, L.; Xia, Y. N. *Adv. Mater.* **2005**, *17*, 473–477.
- (12) Bertling, J.; Blomer, J.; Kummel, R. *Chem.-Ing.-Tech.* **2003**, *75*, 669–678.
- (13) Iida, M.; Sasaki, T.; Watanabe, M. *Chem. Mater.* **1998**, *10*, 3780–3782.
- (14) Schartl, W. *Adv. Mater.* **2000**, *12*, 1899–1908.
- (15) Matijevec, E. *Chem. Mater.* **1993**, *5*, 412–426.
- (16) Gu, S.; Kondo, T.; Mine, E.; Nagao, D.; Kobayashi, Y.; Konno, M. *J. Colloid Interface Sci.* **2004**, *279*, 281–283.

used as exotemplate for the formation of the desired solid and is afterward removed.<sup>10</sup> The last class of syntheses resembles Langmuir–Blodgett techniques, in that the shells are formed by alternately depositing monolayers of poly-electrolyte molecules and inorganic nanoparticles<sup>9,17</sup> (LBL).

Several synthetic paths have been proposed for the preparation of monodisperse core@shell particles with a shell of ZrO<sub>2</sub> or @ZrO<sub>2</sub>.<sup>16,18–24</sup> An interesting double nanocasting approach has been used in ref 20 where in some cases hollow spheres could be synthesized, if the polarity of the precursor was well adjusted. However, the level of control achieved with this method presently seems to be relatively low. Much smaller, nanometer-sized aggregated spheres were claimed to be synthesized by spherical micelle templating.<sup>23</sup> However, they are described to be packed in an ordered array and not isolated entities. A recent report describes emulsion templating for the synthesis of hollow silica-zirconia spheres, which, however, have very thick walls and apparently a relative broad size distribution.<sup>21</sup> In addition, most of these materials show a known problem that is not restricted to special morphologies, but in general seen for mesoporous oxides of the transition-metal oxides:<sup>25–27</sup> as temperature increases, the amorphous oxide structure crystallizes and the crystals growth leads to destruction of the pore structure and disappearance of the high-surface area and the spherical morphology. In addition, the perfection of the spheres is not satisfactory in most cases.

During our attempts to produce hollow zirconia spheres, we have found a method that uses elements of the other types of syntheses and where in addition the silica of the template spheres is partly used as reagent to stabilize the shell. This resulted in the formation of hollow zirconia spheres (containing silicon). These spheres have a number of remarkable features, that is, a very high degree of monodispersity and perfection that is typically not obtained via other pathways, the fact that high temperature stabilization is possible due to the oxidic template sphere instead of a polymer as used in most other approaches, the double role of the template sphere both as template and partly as reagent, and the highly interesting textural properties, such as the very high surface area, of the resulting sphere. Because of these features, the materials described can also be used for the generation of

**Table 1. Description of the Samples Obtained at Different Stages of the Synthesis**

sample	description	step
A	silica sphere	1
B	silica core and amorphous shell with zirconium hydroxide	2
C	silica core and amorphous shell with zirconium hydroxide, aged 3 d at 293 K	3
D	silica core and zirconium oxide shell after calcination at 1173 K	4
E	extraction of silica for different lengths of time	5

more complex structures and replicate into other materials.<sup>28</sup> In the following, the synthesis and the properties of such materials will be described, starting from the synthesis of the zirconia on silica composite, then discussing the creation of the hollow shell material, and finally addressing the thermal stability of the resulting zirconia shells.

## Experimental Section

**Synthesis.** The hollow spheres were synthesized in a five-step procedure (Table 1). First, monodisperse silica spheres were prepared following the well-known Stöber process.<sup>29</sup> The synthesis started by mixing 64 g of ethanol (LiChrosolv, Merck) and 22 g of an aqueous solution of NH<sub>3</sub> (Acros Organics, 28–30%) in a 500 mL flask with one neck. The flask was sealed with a septum, and the solution was heated under stirring to 303 K. Next, 4.2 mL of tetraethoxysilane (TEOS) was rapidly injected into the solution. The system was left to react under stirring for 60 min over which a colloidal suspension containing monodisperse siliceous particles formed. The liquid phase of the colloid was then exchanged for ethanol. This was done by centrifugation (5000 rpm, 5 min), removing the liquid phase, and redispersing the solid in water (100 mL). This step was repeated three times, and then an additional three times by redispersing the solid in 100 mL of ethanol, except in the last centrifugation, where silica spheres were dispersed in 100 g of ethanol (step 1).

In the second step, the monodisperse silica particles dispersed in 100 g of ethanol were poured into a 500 mL single neck flask. Again, the flask was sealed with a septum and heated under stirring to 303 K. Afterward, 0.5 mL of an aqueous solution of 0.43 g of Lutensol AO5, BASF, a nonionic amphiphilic surfactant, in 11 g of H<sub>2</sub>O was added. One hour later followed the addition of 1.8 mL of zirconium butoxide (80 w/w in butanol, Aldrich), and the reaction was allowed to proceed overnight at 303 K. The liquid phase of the colloid was then exchanged for water by centrifugating and redispersing the solid four times in H<sub>2</sub>O (100 mL) (step 2).

Third, the particles were aged in water at 293 K for 3 days. It should be noted here that this step has an important influence on the structure of the shell (step 3).

Fourth, the removal of the organic material and the crystallization of the hydrated zirconia present in the shell into the oxide were achieved during a calcination step under air by heating with a rate of 2 K min<sup>-1</sup> to 1173 K (step 4).

In the final step, the silica from the composite particles was removed by a treatment with sodium hydroxide solution (1 N). First, all samples were kept for 16 h at 303 K in the solution. After the alkaline solution was changed for a fresh one, the extraction was continued for different lengths of time at 323 K. To completely remove the sodium hydroxide solution, the hollow particles were successively filtered, washed five times with H<sub>2</sub>O, three times with

- (17) Caruso, F.; Caruso, R. A.; Möhwald, H. *Science* **1998**, *282*, 1111–1114.  
 (18) Kawahashi, N.; Persson, C.; Matijevic, E. *J. Mater. Chem.* **1991**, *1*, 577–582.  
 (19) Dokoutchaev, A.; James, J. T.; Koene, S. C.; Pathak, S.; Prakash, G. K. S.; Thompson, M. E. *Chem. Mater.* **1999**, *11*, 2389–2399.  
 (20) Dong, A. G.; Ren, N.; Tang, Y.; Wang, Y. J.; Zhang, Y. H.; Hua, W. M.; Gao, Z. *J. Am. Chem. Soc.* **2003**, *125*, 4976–4977.  
 (21) Jiang, Y.; Yang, S.; Ding, X.; Guo, Y.; Bala, H.; Zhao, J.; Yu, K.; Wang, Z. *J. Mater. Chem.* **2005**, *15*, 2041–2046.  
 (22) Xia, Y.; Mokaya, R. *J. Mater. Chem.* **2005**, *15*, 3126–3131.  
 (23) Antonelli, D. M. *Microporous Mesoporous Mater.* **1999**, *28*, 505–510.  
 (24) Yin, J.; Qian, X.; Yin, J.; Shi, M.; Zhang, J.; Zhou, G. *Inorg. Chem. Commun.* **2003**, *6*, 942–945.  
 (25) Schuth, F. *Chem. Mater.* **2001**, *13*, 3184–3195.  
 (26) Soler-Illia, G. J. D.; Sanchez, C.; Lebeau, B.; Patarin, J. *Chem. Rev.* **2002**, *102*, 4093–4138.  
 (27) Taguchi, A.; Schüth, F. *Microporous Mesoporous Mater.* **2005**, *77*, 1–45.  
 (28) Arnal, P. M.; Schüth, F.; Kleitz, F. *Chem. Commun.*, **2006**, *11*, 1203–1205.

- (29) Stöber, W.; Fink, A.; Bohn, E. *J. Colloid Interface Sci.* **1968**, *26*, 62–69.

ethanol, and finally once with ethyl *tert*-butyl ether (50 mL in each wash) (step 5).

**Thermal Treatment.** The hollow spheres were heated in a furnace under ambient atmosphere with a heating rate of  $5 \text{ K min}^{-1}$  to different temperatures and were then cooled to room temperature inside the oven. The calcination temperatures are quoted together with the discussion of the results.

**Nitrogen Sorption Measurements.** The  $\text{N}_2$  sorption measurements were performed on a Micromeritics ASAP 2010 adsorption unit. Prior to the measurements, the calcined samples were activated under vacuum for at least 4 h at 523 K. The measurements were performed at 77 K using a static-volumetric method. The empty volume was determined with helium gas. Textural parameters were determined using the NLDFT kernel of the Autosorb software package provided by Quantachrome, applying as model the adsorption of nitrogen on silica at 77 K.

**X-ray Diffraction Measurements (XRD).** The ex-situ measurements were performed on a STOE STADI P transmission X-ray powder diffractometer using  $\text{Cu K}\alpha_1$  radiation. It is equipped with a linear position sensitive detector. X-ray diffraction patterns were recorded in the ranges of  $20\text{--}35^\circ 2\theta$ .

The crystallite sizes were calculated using the Scherrer algorithm implemented in the Stoe WinX Pow software package. For the particle size calculation, the (111) reflection of tetragonal  $\text{ZrO}_2$  around  $30^\circ 2\theta$  was used.

**Scanning Electron Microscopy (SEM).** The pictures were taken using a Hitachi S-3500N scanning electron microscope (SEM) at 25 kV with a working distance of 5 mm. All samples were deposited on Leit-Tab and were covered with a 10 nm thick layer of gold to improve the image quality.

**Energy Dispersive X-ray Analysis (EDX).** The elemental analyses were performed with an Oxford INCA EDX-System, incorporated into the SEM.

**Transmission Electron Microscopy (TEM).** The pictures were obtained with a Hitachi H-7500 microscope operated at 100 kV. The solid samples were dry deposited on the sample holder (Lacey-carbon, 400 mesh, 3.05 mm) and analyzed without further treatment.

**X-ray Photoelectron Spectroscopy (XPS).** XPS measurements were performed with a Kratos HSi spectrometer with a hemispherical analyzer. The monochromatized  $\text{Al K}\alpha$  X-ray source ( $E = 1486.6 \text{ eV}$ ) was operated at 15 kV and 15 mA. For the narrow scans, an analyzer pass energy of 40 eV was applied. The hybrid mode was used as lens mode. The base pressure in the analysis chamber was  $4 \times 10^{-9}$  Torr. To correct for charging effects, all spectra are referred to C 1s at 285.0 eV.

**Solid-State Nuclear Magnetic Resonance (NMR).** Solid-state NMR spectra were measured on a Bruker Avance 500WB spectrometer using a 4-mm MAS probe at spinning rates of at least 10 kHz. The experimental conditions for  $^{29}\text{Si}$  MAS NMR were 30 s recycle delay, 2400–2800 scans, and  $2.2 \mu\text{s } \pi/4$  pulse. Those for  $^{23}\text{Na}$  MAS NMR were 4 s recycle delay, 400 scans, and  $2.25 \mu\text{s } \pi/4$  pulse. The chemical shifts are given relative to TMS and 1 M NaCl solution for  $^{29}\text{Si}$  and  $^{23}\text{Na}$ , respectively. For  $^{23}\text{Na}$ , solid  $\text{NaNO}_3$  ( $\delta = -8 \text{ ppm}$ ) was used as secondary standard.

## Results and Discussion

**Synthesis of Spherical  $\text{SiO}_2@ZrO_2$ .** Particles consisting of a siliceous core and a porous shell of  $\text{ZrO}_2$ ,  $\text{SiO}_2@ZrO_2$ , were obtained following the synthesis outlined in steps 1–4 described in the Experimental Section.

The specific surface area of the core–shell particles is much higher than the one measured for nonporous silica spheres of similar size. Figure 1a shows a typical nitrogen

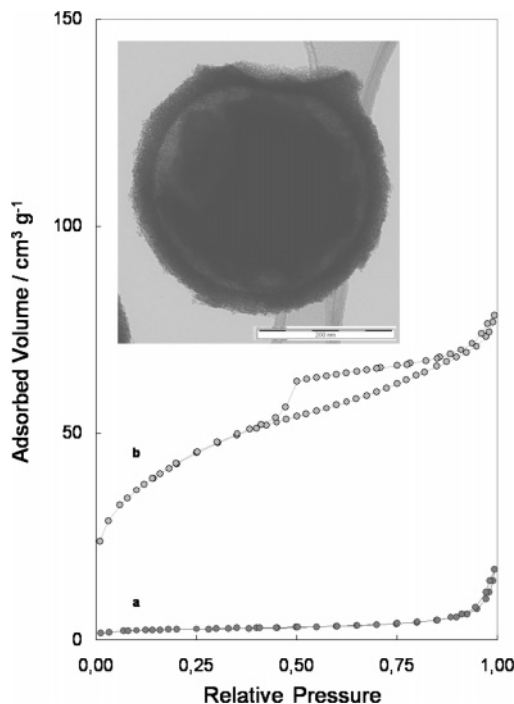


**Figure 1.** Nitrogen sorption isotherms. (a) Monodisperse siliceous spheres; (b) core–shell particles. Inset: TEM image of a core–shell particle.

sorption isotherm of type II for monodisperse silica particles. The isotherm, characteristic for nonporous particles, shows nitrogen uptake at high relative pressures, indicating the occurrence of a capillary condensation of nitrogen in the space between the nonporous silica spheres. In contrast to that, the core–shell particles obtained after step 3 show a sorption isotherm of type IV (Figure 1b) characteristic for materials with a mesoporous structure.<sup>30</sup> The specific area of the silica spheres is  $5 \text{ m}^2 \text{ g}^{-1}$ , corresponding well to the area expected for spherical silica particles with a size of 500–1000 nm and assuming a silica density of  $1.4\text{--}2.0 \text{ g cm}^{-3}$ . The core–shell particles have a specific surface area of  $160 \text{ m}^2 \text{ g}^{-1}$ . This indicates a large contribution of the porous shell to the specific surface area of the core–shell particles. The contribution of the shell alone to the specific surface area can be estimated. As an approximation, we assume that the mass of silica in the core–shell particles can be assessed from the difference of mass between the material before and after the treatment with alkaline solution. The particles lose 44% of their mass. If we neglect the contribution to the surface area from the solid core, the  $160 \text{ m}^2 \text{ g}^{-1}$  measured for the core–shell particles can be attributed to the shell weighing 0.56 g. The shell alone thus has a specific surface area of close to  $300 \text{ m}^2 \text{ g}^{-1}$ .

A clearer picture of the porous structure of the core–shell particles is obtained by NLDFT analysis of the isotherm. The analysis indicates the presence of both micropores and mesopores, the latter having a bimodal distribution with maxima at about 3.0 and 5.2 nm. Additionally, the TEM images show the presence of large cavities (Figure 1b, inset) much bigger than the pores determined by sorption analysis. Before calcination, both the core and the shell are spherical and concentric. A different thermal behavior during calcina-

(30) Schüth, F.; Schmidt, W. *Adv. Mater.* **2002**, *14*, 629–638.

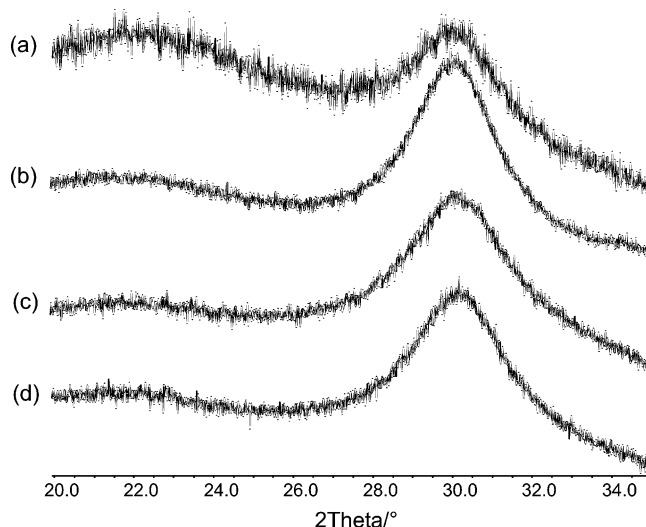


**Figure 2.** XRD results obtained for (a) core-shell particles before extraction and the same material extracted for (b) 23 h, (c) 42 h, and (d) 65 h.

tion leads to a dissimilar expansion and/or contraction of core and shell, which results in the formation of voids between the core and the shell. In addition, the Lutensol, which may have formed an adhesion layer between the inner silica sphere and zirconia layer, is removed during calcinations, which could add to the porosity formed between core and shell, resembling the removal of the polymer layer in ref 16.

Information on the phase composition was obtained from the X-ray powder pattern of the core-shell particles after calcination at 1173 K (Figure 2a). The pattern shows a broad reflection with a maximum at about  $30^\circ 2\theta$ , which is assigned to tetragonal  $\text{ZrO}_2$ . No crystalline  $\text{SiO}_2$  component can be detected. From the analysis of the broad (111)  $\text{ZrO}_2$  reflection using the Scherrer equation,<sup>31</sup> a mean crystallite size of about 5 nm is obtained. This corresponds rather well to the surface area of  $300 \text{ m}^2 \text{ g}^{-1}$  estimated for the shell.

Because XRD analysis does not allow one to obtain structural information on the silica part of the sample,  $^{29}\text{Si}$  MAS NMR experiments were carried out, the results of which are reported in Figure 3. The template silica spheres (trace a) have signals that can be attributed to predominantly  $\text{Q}^3$  (102 ppm) and  $\text{Q}^4$  (111 ppm) silicon atoms. After the aging (step 3) and high-temperature treatment (step 4), the two signals merge into one centered at 109 ppm, which can be assigned to  $\text{Q}^4$  species (trace b). Almost complete condensation of the silica would in fact be expected after treatment at 1173 K.

The bulk composition of the core-shell particles was determined by EDX analysis, and the surface composition was measured by XPS. Both methods reveal the presence of silicon, oxygen, and zirconium. Surprisingly, the zirconium-to-silicon ratio calculated from the XPS data for the surface ( $\text{Zr}/\text{Si} = 1$ ) shows the presence of Silicon also in the shell region. The siliceous particles were completely covered with zirconia during the formation of the shell. Thus, during the aging and/or the calcination process, some of the silicon from the core must have moved into the shell region.

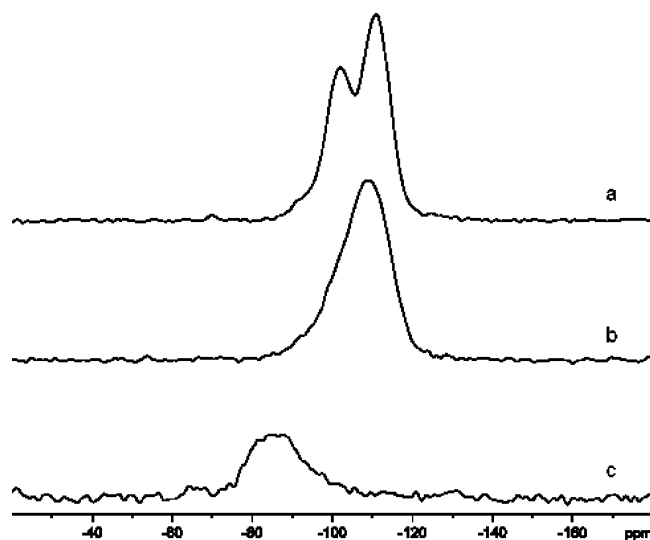


**Figure 3.**  $^{29}\text{Si}$  MAS NMR spectra of (a) monodisperse siliceous spheres (step 1), (b) core-shell particles (step 4), and (c) hollow spheres (step 5).

Summarizing this section, the synthesis and characterization of  $\text{SiO}_2@ZrO_2$  was presented. The monodisperse siliceous spheres used as exotemplates condense and shrink during the thermal treatment in the last step of the synthesis. Nevertheless, a perfectly spherical shell forms, which contains nanometer-sized  $\text{ZrO}_2$  (and silicon) and has a pore structure that gives the material a high specific surface area.

**Hollow Spheres: @ $\text{ZrO}_2$ .** Perfectly shaped spherical hollow particles were obtained after the extraction of the siliceous core with an alkaline solution of sodium hydroxide. The extraction time was varied between 17 and 65 h. Structural and chemical changes during the alkaline treatment were analyzed via XRD, XPS, EDX, nitrogen sorption, TEM, and NMR.

The alkaline solution can reach the interior of the spheres through the porous structure of the shell and dissolves the silica. The XRD patterns of samples extracted for different periods can be seen in Figure 2. The broad feature between  $20^\circ$  and  $25^\circ (2\theta)$  corresponding to the scattering of silica became less intense by increasing the extraction time, although it did not fully disappear. The reflection attributed to  $\text{ZrO}_2$  remains unchanged during the treatment with NaOH solution.

Silicon is only partially removed from the material as shown by chemical analysis. The change of the chemical composition with extraction time is shown in Figure 4a. Before extraction, the zirconium-to-silicon ratio determined for the surface from the XPS data indicates the presence of silicon in the outer region of the spheres. The zirconium-to-silicon ratios for the extracted sample determined both from XPS and from EDX data are higher and in a similar range for both techniques. This indicates a very homogeneous distribution of the elements in the hollow sphere. It is obviously not possible to extract all of the silicon from the sample (Figure 4a); instead, at about 2 the  $\text{Zr}/\text{Si}$  ratio reaches a plateau after an extraction time of about 20 h. The chemical analyses of the extracted samples also revealed the presence of sodium. The sodium had been introduced during the alkaline treatment with NaOH solution. As was already observed for the zirconium-to-silicon ratios, the zirconium-

(31) Scherrer, P. *Gött. Nachr.* **1918**, *2*, 98–100.

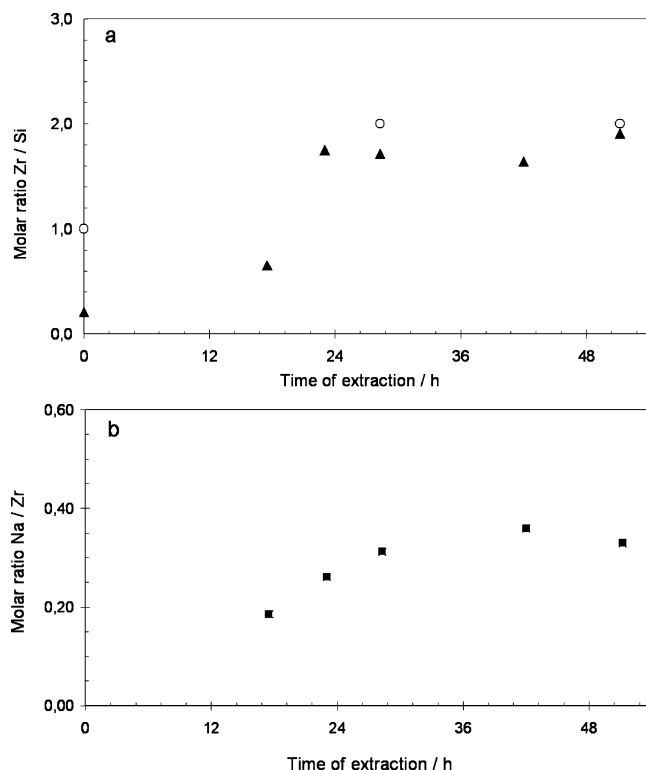


**Figure 4.** (a) Molar ratio of Zr/Si by EDX ( $\blacktriangle$ ) and by XPS ( $\circ$ ), and (b) molar ratio of Na/Zr by EDX ( $\blacksquare$ ).

to-sodium ratios also seem to reach a plateau (Figure 4b). The presence of sodium in the form of residual sodium hydroxide can be excluded on the basis of the  $^{23}\text{Na}$  NMR analysis (not shown). XPS data show one signal for Si as well as for Na and Zr. However, discrimination of different compounds of the same oxidation state is possible by XPS only in fortunate cases, and thus this result does not mean that only one defined compound is present in the materials. For the O 1s spectrum, both an oxidic species and an oxygen species on the surface can be assigned.

The dissolution of the silica component from the core-shell particles leads to an increase of the specific surface area of the spheres (Figure 5). During the extraction, the specific surface areas of the particles approach a final plateau value. Except for the vanishing of the desorption step in the isotherm, the isotherms appear essentially stretched along the adsorbed volume axis, which suggests that the material that does not contribute much to the surface area (the silica core) is removed. The specific surface area calculated for the material after the extraction coincided within the experimental error with the estimated value for the shell in the core-shell particles.

The larger mesopores (5.2 nm) observed for the core-shell particles in the NLDFT analyses disappear during the alkaline treatment. The NLDFT calculation was done with the desorption branch (possible artifact due to ink-bottle effect, see below). By comparing the sorption data with the TEM images (Figure 6), it is obvious that the large mesopores between the core and the shell have disappeared when no silica is present inside the particles. Hence, the siliceous core seems to be related to the hysteresis. The desorption step at  $p/p_0 \approx 0.5$  seems to be related to an “ink-

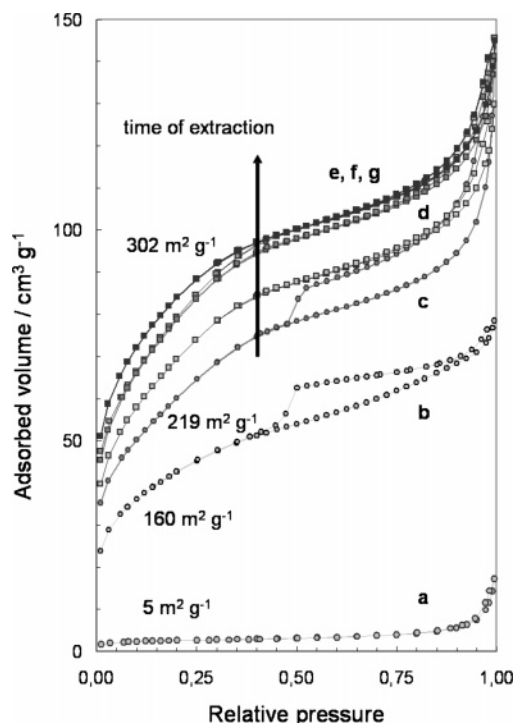


**Figure 5.** Sorption isotherms of monodisperse silica spheres used as template (a), and the core-shell particles extracted for (b) 0 h, (c) 17 h, (d) 23 h, (e) 28 h, (f) 42 h, (g) 51 h, and (f) 65 h.

bottle” or “bottleneck” effect.<sup>32,33</sup> It does not appear any more for the fully hollow shells, because the pressure during adsorption is not high enough to fill the big void in a totally empty shell. Thus, there is no nitrogen in the void that could desorb through the narrow pores of the shell and lead to the desorption step in the isotherm. As a control experiment, pure silica spheres were treated as the composite material up to step 4. However, nitrogen adsorption did not reveal the development of porosity in these materials, and thus the hysteresis and the desorption steps have to be attributed to the fact described above.

After the hysteresis disappears, the isotherms continue their shift toward higher adsorbed volumes (Figure 5, isotherms d, e, f, and g). New micropores and supermicropores appear. This result suggests the dissolution of material from the shell. Nevertheless, the analysis with NLDFT shows only a small change in the porous structure after the alkaline treatment, so that this process does not seem to be very prominent.

The dissolution of the siliceous template can be followed by TEM (Figure 6). Figure 6a shows a core-shell particle before extraction. After 17 h of alkaline treatment, the silica core is partially dissolved in some particles and completely removed in the rest (Figure 6b). The hollow spheres obtained after 65 h are representative for all particles extracted for more than 22 h (Figure 6c). Even after 2 days of treatment in alkaline solution, the secondary structure of the particles remains unchanged.

Provided that the spectra are sufficiently well resolved and the lines are correctly interpreted in terms of  $Q^n$  units ( $\text{Si}(\text{OSi})_n(\text{OH})_{4-n}$ ,  $n = 0-4$ ),  $^{29}\text{Si}$  MAS NMR spectroscopy allows very precise determination of the degree of condensa-

(32) Katz, S. M. *J. Phys. Chem.* **1949**, *53*, 1166–1186.

(33) McBain, J. W. *J. Am. Chem. Soc.* **1935**, *57*, 699–700.

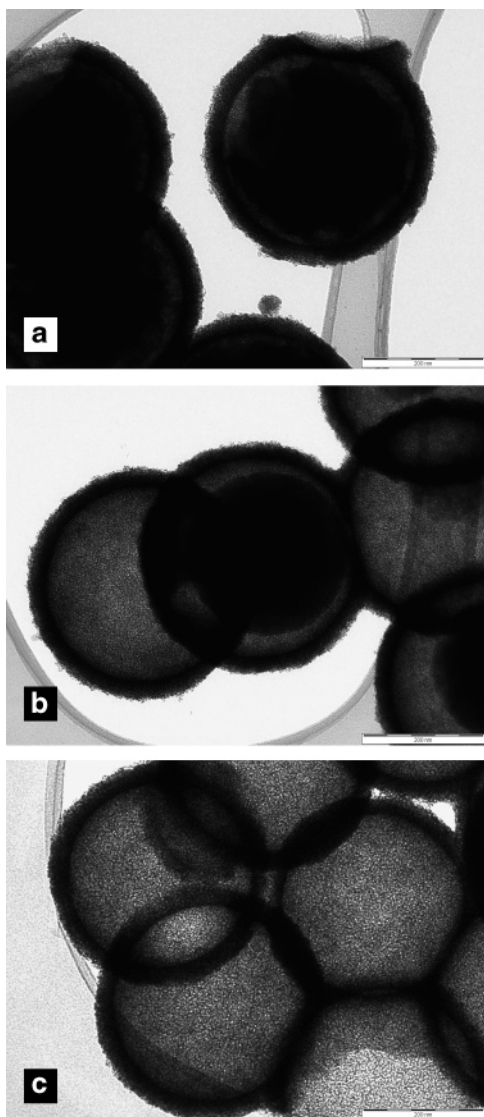


**Figure 6.** TEM images of (a) core-shell particles after calcination (step 4), (b) same material extracted for 17 h, and (c) hollow spheres (step 5). Scale bar 200 nm.

tion in amorphous silicas. However, for thermally treated silicas, usually unresolved asymmetric resonance lines such as those in Figure 3 are obtained. Obviously, the deconvolution of such a line is less reliable.

Furthermore, the ranges of the chemical shift observed for  $Q^n$  groups ( $n = 0, 1, 2$ ) in silicates heavily overlap due to the effect of local geometry and/or counterions.<sup>34</sup> Hence, no assignment to specific  $Q^n$  group can be given for the <sup>29</sup>Si NMR line observed for the extracted sample (Figure 3c). Nevertheless, the obvious difference in the chemical shift before (Figure 3b) and after extraction shows that the degree of condensation of the SiO<sub>4</sub> tetrahedra is significantly changed by this treatment.

On the basis of the experimental evidence, we believe that nanometer-sized particles of ZrO<sub>2</sub>, which are clearly identified by their XRD pattern, are either covered or linked by a siliceous compound different from silica. This compound may contain SiO<sub>4</sub> tetrahedra having a low degree of

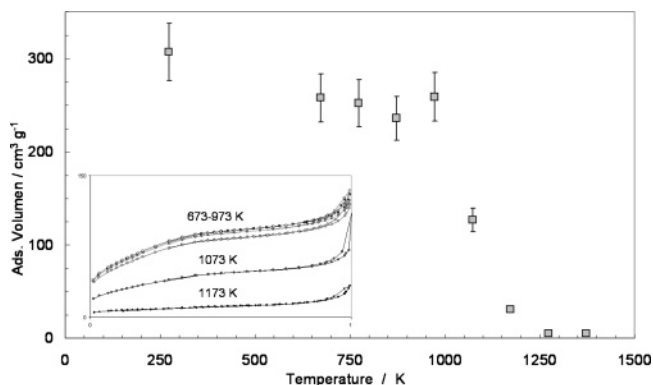


**Figure 7.** Specific surface area of @ZrO<sub>2</sub> thermally treated at different temperatures. Inset: Nitrogen sorption isotherms of the @ZrO<sub>2</sub> treated between 673 and 1173 K.

condensation, sodium and zirconium. It is not probable that it is a pure sodium silicate, because that should not be stable under the leaching conditions. Several materials containing those atoms and a  $Q^n$  ( $n < 2$ ) environment for silicon have been reported,<sup>35</sup> but the available experimental evidence it is not sufficient to determine more precisely the structure of the material.

**Thermal Stability of the Hollow Particles.** High surface area zirconias are especially interesting in high-temperature applications, such as component of washcoat materials in automotive exhaust catalysts. It is therefore important to assess the thermal stability of the materials synthesized.

The morphological and textural changes of the hollow spheres after thermal treatment at different temperatures were followed via nitrogen sorption and SEM. The specific surface area slightly decreases between room temperature and calcination at 673 K (Figure 7). Between 673 and 973 K, the surface area remains more or less constant. Above 973 K, the porous structure of the shells collapses with the corresponding reduction of the specific surface area. The loss of the pore structure is reflected by the strongly decreased amount adsorbed visible in the nitrogen isotherms (Figure 7, inset).

Figure 8a shows an SEM image of spheres calcined at 973 K, which have a porous shell structure. Even though the shell gradually loses its porous structure due to the sintering of the primary ZrO<sub>2</sub> particles, the spherical shape of the secondary particles, the hollow shells, remains unchanged up to 1273 K (Figure 8b,c). Above 1273 K, the secondary particles start to sinter, and their spherical shape is gradually lost (Figure 8d).

The X-ray diffraction patterns of the calcined samples (Figure 9) show that ZrO<sub>2</sub> retains its tetragonal structure up to 1373 K. The presence of tetragonal zirconia after a treatment at such temperature is unusual,<sup>36</sup> but may be due to a stabilization by silicon.<sup>37</sup> Nevertheless, a growth of the nanometer-sized primary crystals can be observed above 1173 K as seen in the narrowing of the reflections. Table 2 shows the mean particle size, calculated from the X-ray

(35) Bastow, T. J.; Hobday, M. E.; Smith, M. E.; Whitfield, H. J. *Solid State Nucl. Magn. Reson.* **1996**, *5*, 293–303.

(36) Stichert, W.; Schüth, F. *Chem. Mater.* **1998**, *10*, 2020–2026.

(37) Wu, N. L.; Wang, S. Y.; Rusakova, I. A. *Science* **1999**, *285*, 1375–1377.

(34) Engelhardt, G.; Michel, D. *High-Resolution Solid-State NMR of Silicates and Zeolites*; John Wiley & Sons: Chichester, 1987.

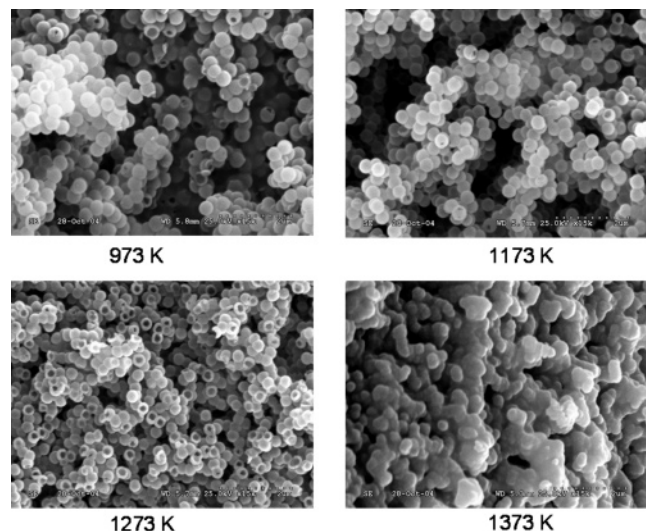


**Figure 8.** SEM pictures showing morphological changes after thermal treatments.

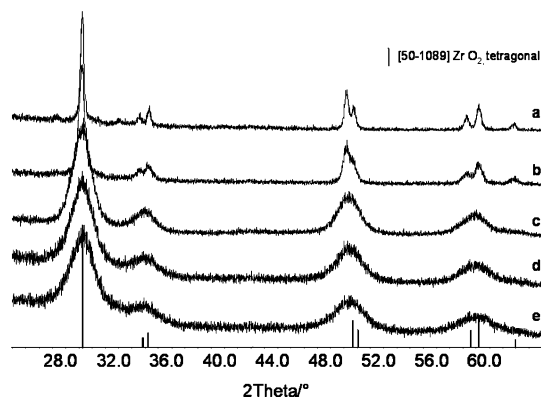


**Figure 9.** XRD patterns of samples calcined at (a) 1373 K, (b) 1273 K, (c) 1173 K, (d) 1073 K, and (e) 973 K.

**Table 2. Particle Size Calculated after Thermal Treatments**

$T/K$	$\langle d \rangle / \text{nm}$	$a / \text{m}^2 \text{g}^{-1}$	$a' / \text{m}^2 \text{g}^{-1}$
973	6	164	259
1073	7	140	127
1173	14	70	31
1273	20	50	<5
1373	35–40	25–28	<5

diffraction patterns, and the expected specific surface area for spherical particles with those sizes ( $a$ ) and the specific surface area calculated from the sorption data ( $a'$ ). There is an obvious discrepancy between the two values after treatment at high temperature. However, one should keep in mind

that sorption analyzes particle sizes with respect to their surface area, while XRD determines the sizes of coherently scattering domains. The discrepancy between the values for the specific surface area calculated both ways may be attributed to the presence of silicon in the system, which could prevent the formation of larger zirconia domains, but at the same time the domains are agglomerated to larger particles, of which the surface area is determined in the sorption experiments.

The XRD pattern for the sample calcined at 1373 K shows additional reflections of a crystalline phase(s), which cannot be assigned unambiguously. However, because both silicon and sodium are present in these samples, there are many nonzirconia phases possible in this system.

First experiments indicate that these materials may have interesting properties as catalyst supports for methanol synthesis and for methanol steam reforming.

## Conclusions

A pathway is described that allows the controlled preparation of monodisperse  $\text{SiO}_2@ZrO_2$  and  $@ZrO_2$  hollow spheres of zirconium oxide. The silica template spheres not only provide a scaffold for the formation of the zirconia, but serve as a source of silicon, which is incorporated in the shell and probably helps to stabilize it.

These hollow spherical particles have a hierarchical structure. The hollow shells are secondary particles, which are composed of nanometer-sized  $ZrO_2$  particles covered and/or linked by a siliceous compound. This compound is X-ray amorphous and contains the elements silicon, oxygen, sodium, and perhaps also zirconium. The exact nature of this phase could not be identified. It may have a crucial role in stabilizing the shells and in maintaining their integrity up to high calcination temperatures.

Possibly, this pathway for the generation of porous shell materials may be extended to other oxides, allowing for the creation of more stable materials as can be prepared by other means.

**Acknowledgment.** We thank Mr. Hans Bongard for the EDX analyses, Mr. Axel Dreier for the TEM analyses, Dr. Bodo Zibrowius for the NMR analyses and thorough interpretation, and Dr. Wolfgang Schmidt for the valuable discussion about the calculation of the pore size distributions from the sorption data.

CM052580A